Lab on a Chip

ROYAL SOCIETY OF CHEMISTRY

PAPER

View Article Online
View Journal | View Issue

Check for updates

Cite this: *Lab Chip*, 2026, **26**, 353

Therapeutic extracellular vesicle preparation *via* sequential electrophoretic enrichment and counterflow microdialysis

Sima Mehraji, [a,c] Nicholas H. Pirolli, [b] Raith Nowak, [b]
Steven M. Jay [b] and Don L. DeVoe *[a,b,c]

Received 12th September 2025,
Accepted 26th November 2025

DOI: 10.1039/d5lc00870k

rsc.li/loc

A microfluidic platform designed to enhance the development of extracellular vesicle (EV)-based therapeutics is presented. The two-chip system combines rapid electrokinetic concentration and purification of EVs together with counterflow buffer exchange to prepare the purified vesicles for pH gradient-driven drug loading. The first chip employs electrophoretic enrichment to capture vesicles at the surface of a nanoporous membrane, with punctuated operation of the electrokinetic device supporting continuous processing of EVs from milliliter-scale volumes of cell culture supernatant. The second chip performs continuous-flow buffer exchange to protonate the vesicles and form a transmembrane pH gradient prior to passive loading of nucleic acid cargo. The modular components are shown to preserve EV bioactivity throughout the full process, using disposable thermoplastic chips that eliminate the need for device cleaning or regeneration between process runs. The technology enables a rapid and convenient workflow for EV-based therapeutic development addressing key limitations associated with established batch processes.

Introduction

Due to their biocompatibility, nanoscale dimensions, and intrinsic targeting capabilities, therapeutics employing extracellular vesicles (EVs) as drug carriers have garnered substantial interest in recent years.[1] As the field advances, there is a need for improved EV therapeutic development workflows that can accelerate preclinical studies and early clinical trials.[2,3] Regardless of the vesicle source, *e.g.* patient tissues or cell culture, vesicle purification,[4,5] concentration,[5–7] and cargo loading[8–11] are central steps for the preparation of EV-based nanomedicines. Faster and more efficient methods for vesicle enrichment, contaminant removal, and drug loading are thus essential to fully harness the potential of EVs for drug delivery.

Current approaches for the isolation and enrichment of EVs prior to downstream drug loading typically employ ultracentrifugation,[12–14] tangential flow filtration (TFF),[15,16] size exclusion chromatography (SEC),[17,18] affinity-based isolation[19] or a combination of these techniques.[20] While ultracentrifugation is accessible and capable of processing large volumes, the high inertial forces can disrupt vesicles and co-pellet proteins, thereby reducing EV yield and requiring additional processing steps to ensure product purity.[21] In addition, centrifugation is a batch process that not amenable to scalable manufacturing using continuous-flow processing. SEC can effectively isolate EVs from proteins based on size in a gentle process that avoids vesicle degradation, but it can suffer from low recovery, limited throughput, and high variability. SEC also requires the use of resins that must be periodically regenerated and replaced,[17] and like UC it also suffers from poor scalability. While TFF is a continuous-flow process that is fully scalable while offering high yield and reproducibility, it often retains larger soluble protein contaminants, and employs infrastructure that requires specialized training to operate and maintain.[22,23] Unlike size- or charge-based techniques, affinity-based isolation captures vesicles through specific molecular recognition, enabling highly selective purification of target EV subpopulations.[19,24,25] However, this approach can suffer from low recovery, high reagent costs, potential alteration of vesicle surface properties during elution, and poor scalability for therapeutic EV production.[22,26] Precipitation-based purification of EVs has been widely employed[22,24] as a low cost and highly scalable process.[27,28] However, precipitation is slow (>12 h) and results in co-precipitation of non-EV components that reduce the purity of the final solution.[29]

---

[a] *Department of Mechanical Engineering, University of Maryland, College Park, MD, USA. E-mail: ddev@umd.edu*
[b] *Fischell Department of Bioengineering, University of Maryland, College Park, MD, USA*
[c] *Fischell Institute for Biomedical Devices, University of Maryland, College Park, MD, USA*

To overcome these various limitations, a number of microfluidic platforms have emerged as promising tools for EV processing.[30–32] Passive size-based microfluidic systems based on deterministic lateral displacement (DLD) have been shown to enable the removal of large particles during continuous flow while preserving EVs under low-shear conditions.[33,34] Platforms employing low-volume membrane filtration based on direct size exclusion[35,36] or microfluidic TFF[15] have also been developed with high levels of EV purification and recovery reported. However, these passive microfluidic systems are tailored for EV biomarker discovery or detection from small sample volumes rather than scalable therapeutic development.

In contrast to these passive technologies, active processing using electrokinetics offers potential for enhancing both the selectivity and throughout for EV enrichment by leveraging the well-defined charge state and dielectric properties of the vesicles.[37] Microfluidic platforms based on dielectrophoresis (DEP) have used the polarizability of EVs to capture vesicles within the nonlinear electric field gradient at the edges of a fixed electrode,[38] while also platforms have employed an array of DEP electrodes within a flow cell to selectively route vesicles to a collection channel while allowing proteins and other contaminants to be depleted from the initial suspension.[39–41] Extending this latter approach, DEP has been further combined with acoustophoresis to sort EVs with 95% purity and 81% recovery.[40] Ion concentration polarization (ICP) has also been explored for EV enrichment by electrokinetically mobilizing the charged vesicles toward an ion-selective membrane where a local ion depletion zone creates a barrier to further transport, resulting in vesicle accumulation at the membrane surface.[42–44] While ICP has been shown to enable EV enrichment with higher recovery and lower vesicle damage than UC,[45] the process is constrained by the use of static sample volumes[44] or low flow rates on the order of 1–3 μL min^{-1},[43,45] together with low overall loading capacity due to small membrane surface area, limiting its utility for scalable therapeutic processing.

Beyond DEP and ICP, a number of other microfluidic platforms have combined electrophoresis with membrane filtration for EV processing. Because EVs possess a negative charge, they are readily mobilized by direct electrophoresis within an electric field. By imposing a voltage gradient across a membrane while passing EVs through an adjacent microchannel, vesicles may be mobilized through the membrane pores while rejecting larger contaminants by size exclusion. While electrophoretic filtration has been demonstrated for EV purification from blood using a porous polymer monolith integrated into a thermoplastic chip,[46] this approach cannot remove proteins or other contaminants below the membrane pore size. Alternately, by using a membrane with pore dimensions below the minimum EV size, vesicles may be retained and concentration on the membrane surface while charged contaminants are allowed to traverse the pores. This electrophoretic enrichment process has previously implemented in a millifluidic system fabricated from machined aluminum, with a pair of track-etched polycarbonate membranes separating a sample flow channel from upper and lower buffer chambers containing electrode plates[47] When applying a transverse electric field across the sample channel, 60% EV recovery and 84% protein removal was achieved under 20 μL min^{-1} continuous sample flow.

Following EV concentration and purification, the efficient loading of drug cargo into the enriched vesicles presents a further bottleneck in the development of EV-based therapeutics.[8,48] Batch methods employing mechanisms including electroporation,[49] sonication[50] are widely employed to disrupt the membrane to enable the diffusion of nucleic acids or small molecules into the vesicles. While the literature documents successes with this method, other studies have raised concerns, noting issues such as significant RNA aggregation and alterations in EV morphology.[51] Another study reported that sonication enables siRNA loading without notable aggregation, although extended sonication times led to nucleic acid degradation.[52] In this context, pH gradient-driven loading of nucleic acids is a recent advance for EV therapeutic preparation enabling loading efficiencies comparable to methods based on membrane disruption while avoiding vesicle or cargo degradation.[53–56] The pH gradient loading process works by protonating the internal lumen of the vesicles, resulting in electrostatic interactions with therapeutic molecules such as microRNA (miRNA) or small interfering RNA (siRNA that are able to draw these small negatively-charged nucleic acids into the vesicle core. However, the technique remains a batch process requiring multiple steps including dehydration, rehydration, dialysis, and drug incubation that are not amenable to in-line processing. To improve the reliability and throughout while reducing reliance on complex instruments, new technologies are needed to move key steps of the pH gradient drug loading process towards continuous-flow operation.

Here we introduce a two-chip microfluidic platform designed to address several of the central challenges in EV-based therapeutic development. The platform was validated using EVs isolated from cell culture supernatant, rather than clinical specimens or biofluids, as a common source of vesicles employed in typical EV drug production pipelines. A schematic of the multi-chip EV processing workflow is shown in Fig. 1. The first chip combines electrophoresis-assisted EV enrichment and purification from cell culture supernatant to enable over 100-fold increase in the ratio of EVs to total protein, while recovering more than 70% of the processed vesicles. The second chip performs pH gradient-driven buffer exchange to prepare the EVs for therapeutic nucleic acid loading, and is shown to support efficient passive loading of siRNA cargo. The thermoplastic chips integrate commercially-available membranes, and are designed as disposable components to avoid the need for routine sterilization or membrane replacement while reducing the cost and complexity associated with conventional workflows.

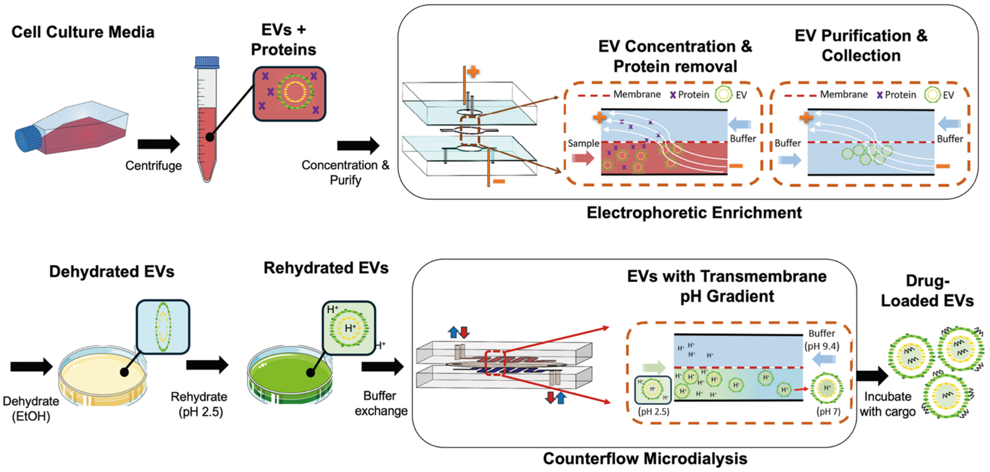

Fig. 1 Microfluidic-enabled workflow employing an electrophoretic enrichment chip enabling concentration and purification of EVs from cell culture media, and a counterflow microdialysis chip supporting transmembrane pH gradient generation to prepare EVs for drug loading.

Both chips operate in a continuous flow-through format, providing a compact and modular solution to advance EV therapeutic development.

Materials and methods

Electrophoretic filtration chip fabrication

A summary of the fabrication process used for the electrophoretic filtration device is illustrated in Fig. 2. The design consists of an upper buffer chamber and lower sample perfusion chamber separated by a hydrophilic mixed cellulose ester (MCE) membrane (0.025 μm pore size, 72% porosity, 25 mm diameter; MF-Millipore). The high membrane porosity serves to minimize voltage drop across the membrane for reduced Joule heating of captured vesicles while also enhancing mass loading and protein filtration. The membrane was patterned using a cutter plotter (Cameo 4, Silhouette) to form an 11 mm diameter central circular region with two 4.5 mm wide and 7 mm long side extensions that align to channels in the lower sample perfusion layer. The membrane was patterned to increase the available bonding area to ensure leak-free operation. The buffer and sample perfusion layers were each constructed from a 1.6 mm thick polycarbonate (PC) substrate laser-cut to 1.5 × 3 cm and drilled with 0.65 mm diameter holes to create inlet, outlet, and electrode wire access ports. Fluidic channel geometries were defined using a double-sided pressure-sensitive PET adhesive film (ARcare 90445Q, Adhesives Research; total thickness: 81 μm), patterned using a cutter plotter (Cameo 4, Silhouette) to form a 9 mm diameter central circular channel connected to two 1.5 mm wide side and 5.5 mm long channels in the bottom layer, and a 9 mm diameter circular chamber in the top layer. The MCE membrane was placed between the two PC/PET films to separate the sample media (bottom) and buffer (top) chambers. After precise alignment, the full stack was compressed in a benchtop hydraulic press (Dabpress) at 400 psi for 4 min to bond the layers and seal the channels. After bonding, the total on-chip volume within the sample flow path was approximately 6.5 μL. Finally, 1 in long 22 gauge blunt-tip stainless steel needle segments (Hamilton Syringe) were inserted into the inlet and outlet ports for fluidic interfacing, with 500 μm i.d. flexible tubing (Microbore, Tygon) connecting the inlet and outlet needles to a syringe pump and sample collection vial, respectively. The total dead volume associated with the needle ports and tubing is estimated to be 20 μL. Nickel–chromium alloy wires (NiCr 80/20, 22 gauge, Master Wire Supply) were inserted through two ports located in the buffer chamber and near the inlet of the sample perfusion channel as integrated electrodes for electrophoretic operation, with 7.5 mm lateral spacing between the ports. To ensure a leak-proof assembly, the electrode access holes were sealed using epoxy.

Microdialysis chip fabrication

The microfluidic microdialysis devices used to prepare EVs for drug loading following electrophoretic enrichment and purification employed a fabrication process similar to the electrokinetic concentration chips, but with multiple layer stacked on top of one another to increase the overall length of the dialysis zone.[57] Briefly, each layer was fabricated with a sample flow channel and buffer counterflow channel separated by a 2.5 cm diameter MCE dialysis membrane (0.025 μm pore size). Serpentine microchannels, each 1.5 mm wide and 12.5 cm long, were patterned in adhesive PET sheets. A pair of patterned PET layers were bonded to opposite sides of an MCE membrane, and PC substrates were bonded to each of the exposed PET surfaces to enclose the microchannels, thereby defining sample and buffer flow paths. This process was repeated to yield the full 4-layer device, with holes (1.5 mm diameter) formed in the membrane using a biopsy punch (Miltex) and in the PC substrate using a drill press to create interlayer connections

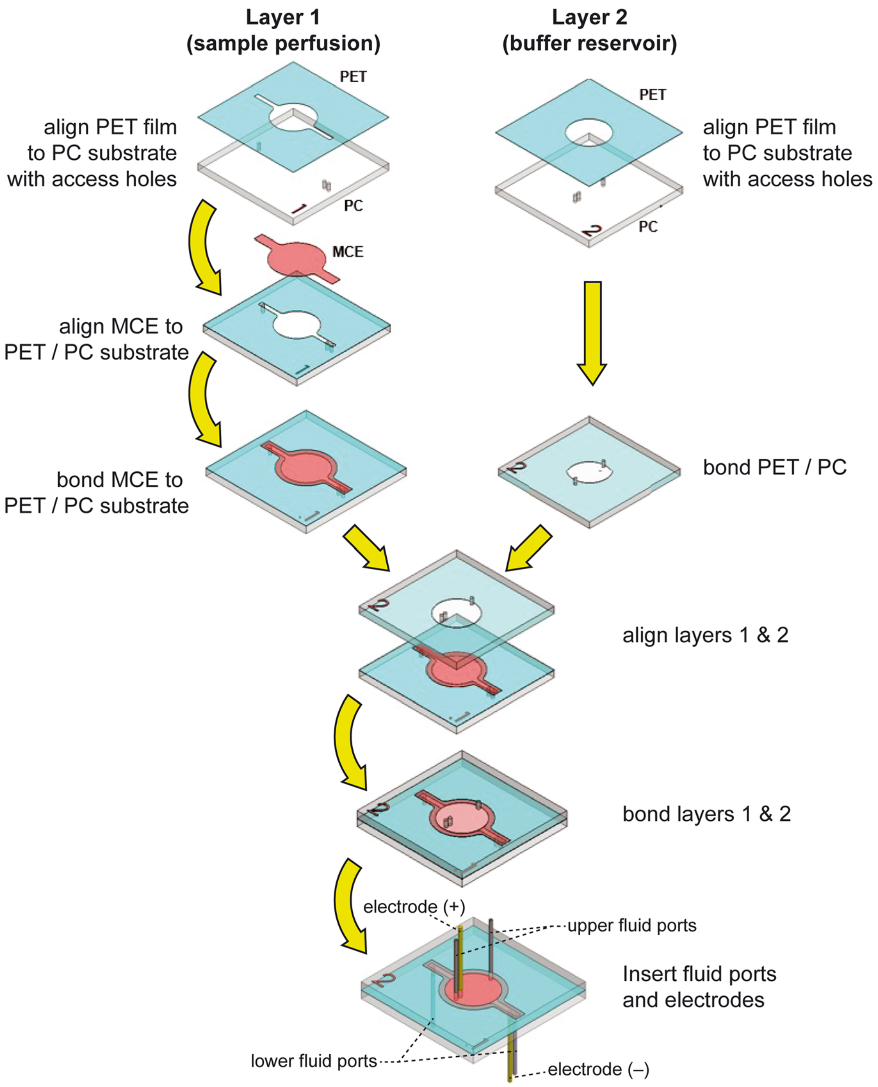

Fig. 2 Fabrication process for the electrokinetic chips for EV concentration and purification. Adhesive PET tape layers are used to define the channel and reservoir geometry, and bonded with polycarbonate substrates containing pre-drilled holes for fluidic and electrical interfacing. A patterned MCE membrane is positioned between the mating PET/PC layers. Needle ports and electrodes are inserted into the PC layers after bonding.

allowing fluid flow between adjacent layers. After alignment and assembly of the multilayer stack, the device was compressed in a benchtop hydraulic press to permanently bond the layers. Blunt-tip needle segments were used as inlet and outlet ports for both sample and counterflow buffer in the final device.

Numerical simulations

The behavior of EV particles during electrophoretic enrichment was investigated through numerical simulations developed in COMSOL Multiphysics 6. The particle tracing module was employed to model EV trajectories, with the 3D model constructed with the dimensions of the fabricated device. The simulations employed the electric currents and creeping flow interfaces to capture the electrokinetic environment and the low-Reynolds-number fluid dynamics characteristic of the system, respectively. The simulations were performed using an electrophoretic mobility for the particles given by 1.2×10^{-4} cm^2 V^{-1} s^{-1}. This value was selected since 95% of the vesicles exhibited EV mobility values greater than this lower limit (Fig. S1).

Cell culture and sample preparation

Human embryonic kidney (HEK293T; ATCC CRL-3216) cells were cultured in Dulbecco's modified Eagle's medium (DMEM) [+] 4.5 g L^{-1} glucose, L-glutamine, and sodium pyruvate (10-013-CV; Corning, NY, USA), supplemented with 10% fetal bovine serum (FBS) and 1% penicillin–streptomycin, in T-175 tissue culture flasks. Human mesenchymal stem cells (hMSCs) were similarly maintained in DMEM supplemented with 10% FBS (Cytiva; SH30910.03), 1% penicillin–streptomycin (VWR; 45000-652), and 1% nonessential amino acids (Thermo Fisher Scientific; 11140050). To remove serum-derived EVs, complete media was depleted using tangential flow filtration (TFF) through a 300 kDa filter, where the permeate was collected and the retentate discarded. Cells were cultured to approximately 50% confluency, washed with PBS, and then cultured in the EV-depleted media for 24 hours. The conditioned media was then collected and subjected to differential centrifugation at 1000 × *g* for 10 min, 2000 × *g* for 20 min, and 10 000 × *g* for 30 min, retaining only the supernatant after each spin for subsequent processing.

EV enrichment and purification

A schematic of the complete EV processing workflow and integrated microfluidic platform is shown in Fig. 1. HEK-conditioned media was first clarified by sequential centrifugation at 1000 × *g* for 10 min, 2000 × *g* for 20 min, and 10 000 × *g* for 30 min to remove cells and large debris. The resulting supernatant, containing EVs at concentrations in the range of 10^8–10^{10} particles per mL, was introduced into the electrophoretic filtration chip. In this module, the sample was infused through the top (sample) chamber at a flow rate of 10 μL min^{-1}, while 1× PBS was introduced into the bottom (buffer) chamber at the same flow rate. An electric field was applied across the membrane by connecting the anode to the wire at the sample inlet and the cathode to the buffer chamber wire. Upon applying a DC bias in the range of 45–75 V, EVs were electrophoretically concentrated at the bottom surface of the nanoporous membrane, while negatively-charged proteins and small contaminants were allowed to migrate into the buffer chamber. After concentrating vesicles for time periods up to 40 min, the sample channel was flushed with 1× PBS for 5 min at 7 μL min^{-1} while maintaining the electric field to displace residual media with buffer while retaining collected EVs at the membrane surface. The voltage was then turned off, and purified, enriched EVs were collected for downstream processing by perfusing 100 μL of buffer through the system.

Buffer exchange

For pH-gradient preparation,[56] the concentrated EVs were suspended in 70% ethanol (prepared by combining 700 μL of 100% ethanol with PBS) to a final concentration of 300 μg mL^{-1} and left to dehydrate overnight (~12 hours) in a 24-well plate. Following evaporation of the ethanol, 1 mL of 300 mmol L^{-1} citrate buffer (pH 2.5) was added to rehydrate the EVs, and the solution was gently agitated at room temperature for 1 h. The rehydrated EVs were then introduced into the 4-layer microdialysis chip for rapid ion exchange. The HBS stock was prepared by dissolving 43.8 g of NaCl in 400 mL of Milli-Q water and adding 100 mL of 1 M HEPES. HEPES-buffered saline (HBS; pH 9.4) was flowed through the counterflow inlet in the opposite direction. The system was operated for at least twice the calculated residence time to ensure full establishment of the transmembrane pH gradient. Outlet samples were collected and analyzed to confirm a pH shift from 2.5 to 7.0 across the exchange membrane.

For control EV preparations, ultracentrifugation was employed. Following differential spins, the conditioned media was filtered through a 0.2 μm vacuum filter. EVs were then isolated from the conditioned media *via* tangential flow filtration (TFF) in a KrosFlo KR2i TFF system (Repligen; Boston, MA, USA). A 300 kDa MWCO MidiKros membrane (D02-E300-05-N; Repligen, Boston, MA, USA) was utilized for filtering with a transmembrane pressure of 5 psi. The conditioned media was concentrated to 20 mL before 15 diafiltration volumes of PBS were used to wash the samples before a final concentration down to 10 mL. The samples were further concentrated to ~1 mL using a 100 kDa Spin-X UF Concentrator (431486; CORNING, Corning, NY, USA) before syringe filtering with a 0.2 um filter and storing at −20 °C.

EV loading

The enriched and pH gradient-modified EVs were incubated with 0.25 mg mL^{-1} acridine orange (AO) in HEPES buffer for 1 h to evaluate loading efficiency. Multiple samples were collected for each test ($n = 3$). To ensure that residual free AO in the collection buffer did not interfere with concentration measurements, the loaded EV samples were dialyzed against isosmotic HEPES buffer using 300 kDa molecular-weight-cutoff dialysis units (Float-A-Lyzer G2; SpectraPor, USA). Dialysis was performed for 4 h with 3 buffer exchanges to ensure complete removal of unencapsulated dye. Following purification, absorbance measurements of the dialyzed samples and a serial dilution of AO standards were obtained at λ_{max} = 495 nm using a spectrophotometer (SmartSpec 3000, Bio-Rad Laboratories, USA). Absorbance values were compared with the standard calibration curve to determine the final encapsulated AO concentration.

EV characterization

Size distribution and particle concentration were assessed by nanoparticle tracking analysis (NTA) using a NanoSight LM10 (Malvern Instruments) with NTA analytical software version 3.4. Individual EV samples were diluted as necessary (typically 500×) to obtain between 20–100 particles per frame and at least 200 completed tracks per video to ensure accurate analysis. For each sample, three 30 s videos were captured with a camera level set at 14. The detection threshold was set at 3 and kept constant across all replicates and samples. Total protein concentration in each EV sample was determined using a bicinchoninic acid (BCA) assay kit (G-Biosciences).

Western blots

To confirm EV presence in the isolated sample and not the waste, western blots were performed on the common EV marker CD63. Protein content of samples collected from media waste, buffer waste, isolated EVs, and conditioned media was quantified using a bicinchoninic acid (BCA) assay. Additionally, a sample of EVs isolated by TFF was added as a control for EV presence, along with loading 200 μg of conditioned media. CD63 presence was assessed by staining the western blot membrane with a rabbit anti-human CD63 primary antibody (Proteintech 25682-1-AP) at a 1:1000 dilution. An anti-rabbit goat secondary antibody (LI-COR Biosciences 926-32211) was then added at a 1:10000 dilution for imaging. Protein band imaging was performed on a LI-COR Odyssey CLX.

Macrophage inflammatory assay

RAW264.7 murine macrophages were seeded at 7.5 × 10^4 cells per well in 48-well plates containing DMEM supplemented with 10% fetal bovine serum and 1% penicillin–streptomycin. After a 24 h attachment period, cells were pretreated (in triplicate) with one of the following conditions: phosphate-buffered saline (PBS), EV-containing conditioned medium, 1 μg mL^{-1} dexamethasone as a positive anti-inflammatory control, and EVs processed through electrokinetic concentration and pH-gradient buffer exchange, normalized by particle count to 1×10^8, 1×10^9, and 1×10^{10} particle doses. Following 24 h pretreatment, the media was removed and replaced with 10 ng mL^{-1} lipopolysaccharide (LPS, *E. coli* O111:B4, Sigma Aldrich) in PBS, except for 3 PBS-treated wells serving as unstimulated controls. After 4 h of LPS stimulation, supernatants were collected, snap-frozen at −80 °C, and analyzed for TNF-α levels using ELISA within 3 days.

Results and discussion

Electrophoretic concentration

Extracellular vesicles possess a net negative surface charge due primarily to the presence of glycoproteins as well as both anionic and zwitterionic phospholipids in their membranes,[58] As a result, EVs can exhibit high electrokinetic mobility and will migrate in a direction opposite to an applied electric field. The microfluidic electrokinetic concentration device reported here imposes a positive field between a sealed upper buffer reservoir and a lower sample channel separated by a membrane with pore dimensions of 25 nm, below the 30–40 nm EV size limit.[59,60] When the electrokinetic drift velocity is sufficient to overcome bulk fluid flow, vesicles are retained at the membrane surface before exiting the chamber, allowing EV concentration to increase over time as sample is perfused through the system.

Using a fabricated electrophoretic enrichment chip as presented in Fig. 3A, vesicle retention was evaluated under varying voltages, operation times, and initial EV concentrations to assess device performance and identify optimal operational parameters. As shown in Fig. S2, experiments were performed at an operating voltage of 75 V to investigate the effect of flow rate. As flow rate increases, a greater portion of EVs is able to escape the collection chamber due to higher average hydrodynamic mobility,

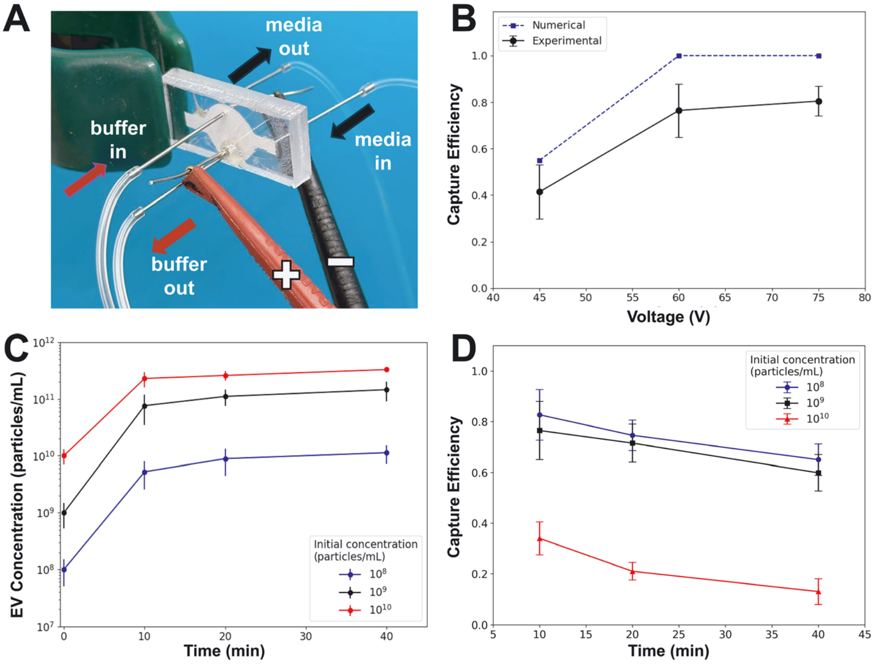

Fig. 3 EV concentration performance under varying voltages and processing times. (A) Fabricated microfluidic flow cell with integrated electrodes and MCE membrane for electrophoretic enrichment and purification of EVs. (B) Effect of applied voltage on EV retention during electrokinetic capture. Experimental data was collected using an input solution of 1×10^9 vesicles per mL and 10 min capture period. (C) Time-dependent concentrations and (D) capture efficiency for initial EV input levels between 10^8–10^{10} vesicles per mL when operating at 60 V bias. All experiments were performed at a constant flow rate of 10 μL min^{-1}.

resulting in a drop in EV recovery. Based on these results, a flow rate of 10 μL min^{-1} was selected for subsequent studies. A numerical model (Fig. S3) was employed to evaluate the electric field distribution, with particle tracing used to determine vesicle capture efficiency, defined as the number of EVs retained in the collection chamber normalized to the total number of vesicles perfused through the system at each time point. As expected, electric field distribution within the enrichment chamber was found to be highly inhomogeneous for the given chamber geometry, electrode geometry, and electrode positions. The simulated EV particles were found to aggregate at the lower membrane surface immediately beneath the buffer electrode and at the interface between the collection chamber and outlet channel, with an increasing portion of the captured particles appearing near the electrode at higher voltages. While the single-wire electrodes used in our design served to simply device fabrication, further efforts to optimize system performance would likely benefit from the use of multiple buffer electrode wires or integration of a single large cathode at the upper surface of the buffer chamber to enhance electrokinetic mobilization of EVs to the membrane surface.

As seen in Fig. 3B, the numerical model predicts complete capture at voltages above 60 V, whereas at 45 V the device retains only 56% of vesicles introduced into the system. A similar trend was observed in experimental data collected using an input concentration of 10^9 particles mL^{-1} (Q = 10 μL min^{-1}, t = 10 min), although with reduced capture efficiency that plateaus at a value around 75% at biases above 60 V. The lower measured peak capture efficiency may reflect losses during the EV recovery and measurement process. Vesicle loss may also result from particle degradation due to Joule heating, particularly at higher applied voltages. The electrothermal response of the sample solution during enrichment was also modeled by numerical simulation, yielding a steady-state peak temperature rise of 14 °C when employing a 60 V bias. Although EVs have been shown to exhibit a high level of physicochemical stability at 37 °C for at least 24 h, temperatures of 50 °C and beyond can lead to vesicle degradation.[61] Thus while the impact of Joule heating on vesicle loss is expected to be minimal at 60 V, higher biases may impact performance. To reduce the potential for vesicle degradation while maximizing capture efficiency, a bias of 60 V was selected for all subsequent experiments. The effect of processing time on vesicle capture was next examined across a range of initial EV concentrations (10^8, 10^9, and 10^{10} particles per mL) at 60 V and Q = 10 μL min^{-1}. Under these conditions the steady-state current was measured as 1.25 mA, with a nearly linear current–voltage relationship observed when gradually increasing the voltage up to 60 V, suggesting minimal contribution of electrochemical or nonlinear polarization effects to the overall electric field within the device.

As expected, longer capture times resulted in higher EV concentration in the final eluent (Fig. 3C). However, as seen in Fig. 3D, capture efficiency was found to drop longer operating times and initial vesicle concentration, with a significant reduction in capture efficiency observed as the initial sample concentration increases from 10^9 to 10^{10} EV mL^{-1}. This behavior is likely due to limited membrane capacity, with disruption of the electric field gradient and reduced electrokinetic velocity occurring as larger numbers of vesicles accumulate in the available membrane pores. The formation of an osmotic pressure gradient may also play a role, with transport of ions across the membrane during vesicle enrichment generating a bulk fluid flow that opposes mobilization of EVs to the membrane surface.

To confirm EV enrichment using an orthogonal assay, Western blots were performed to measure levels of CD63 as an EV biomarker[62] in enriched sample, culture media waste, and buffer waste from an electrokinetic chip following 10 min capture at 60 V and 10 μL min^{-1} flow rate (Fig. S5). Assays were also performed with initial culture medium as well as TFF-processed culture medium as a comparative control. No detectable marker was found in the buffer waste, while a clear set of bands reflecting the presence of CD63 and its glycosylated isoforms were observed in the initial culture medium and enriched sample. The primary band intensity for the enriched sample was found to be approximately 20% lower than the initial culture media band, consistent with the collection efficiency results previously obtained by DLS analysis (Fig. 3D), while quantification of the culture medium waste reveals approximately 8% EV loss relative to the initial culture medium. This discrepancy is most likely due to the semi-quantitative nature of the Western blots, although it is also possible that some vesicles remain trapped within the membrane pores or irreversibly adsorbed to the membrane or channel surfaces. We also note that the lack of CD63 in the buffer waste suggests that no significant passage of EVs or vesicular debris across the membrane occurs during enrichment.

Given a nominal concentration of 1 × 10^9 particles per mL for our EV samples harvested from HEC cell culture, an

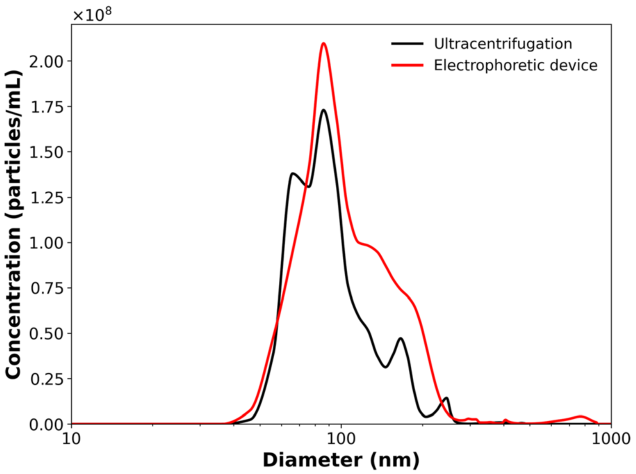

Fig. 4 Particle size distributions after enrichment by conventional ultracentrifugation, and after microfluidic electrophoretic enrichment at 10 μL min^{-1} flow rate and 60 V bias for 10 min.

electrophoretic concentration time of 10 min at 60 V was used for following studies to avoid significant saturation while concentrating EVs to final levels suitable for pH gradient-mediated cargo loading (~10^{11} particles per mL).[61]

EV recovery and size distribution

Size distribution analysis revealed effective EV enrichment by the electrokinetic concentrator compared with ultracentrifugation (Fig. 4). All experiments yielded a dominant peak centered near 86 nm and an overall particle size distribution between approximately 50–200 nm as expected for the purified EV samples. The microfluidic device achieved a peak particle concentration nearly 20% higher than ultracentrifugation, and over 40% higher total vesicle recovery based on the area under each curve, revealing that the electrokinetic mechanism is capable of capturing a greater portion of the vesicle population while minimizing loss during processing. Additionally, both the conventional and microfluidic methods significantly reduced a secondary peak near 140 nm observed in the untreated HEK-conditioned media (Fig. S4) that may reflect the presence of protein aggregates, apoptotic bodies, or other non-vesicular debris in the initial sample.

Protein removal efficiency

Depleting proteins during the preparation of EV-based therapeutics is necessary to ensure safety and efficacy of the final drug product, since residual proteins can obscure the therapeutic effects of EVs and trigger unwanted immune responses. Because the 25 nm pore size of the membrane used for electrokinetic concentration is significantly greater than the hydrodynamic radius of most proteins, including large antibodies such as IgM, negatively charged proteins are expected to be efficiently transported across the membrane during the EV concentration process, while proteins carrying a net positive charge are electrokinetically ejected from the concentration zone. Protein removal was evaluated using a BCA assay, both with and without a post-processing PBS flush prior to EV collection. As shown in Fig. 5, the ratio of EVs to total protein increased by more than 100-fold in the enriched sample compared to the initial culture medium and other control samples. While conventional approaches to protein removal such as tangential flow filtration (TFF),[63] ultracentrifugation,[12] and bulk dialysis[64] typically require large sample volumes and extended operation times, the electrophoretic device achieves comparable protein depletion and buffer replacement while processing smaller sample volumes (100 μL) in a convenient and rapid flow-through process, making it particularly well-suited for preclinical studies or work using limited EV samples.

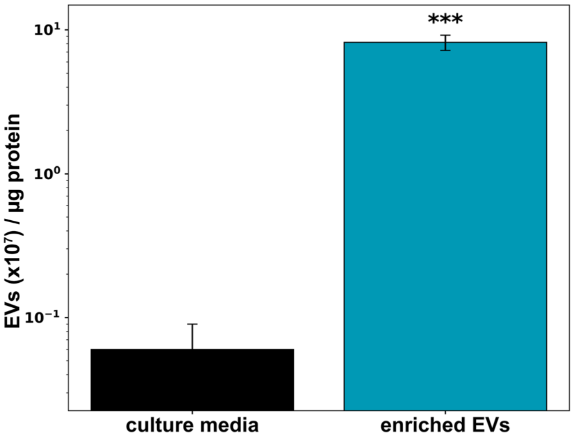

Fig. 5 Number of HEK293T EVs per microgram of protein measured in initial culture media and processed samples following electrokinetic enrichment (*n* = 3). EV counts and protein amounts were determined by NTA and BCA analysis, respectively.

Punctuated sample enrichment

Due to the saturation effect observed in Fig. 3C, the electrophoretic enrichment process cannot be applied to arbitrarily large sample volumes without loss of performance. To overcome this limitation while enabling continuous and scalable processing, operation of the device in a punctuated mode was explored. In this approach, large samples are processed by sequentially concentrating and collecting smaller aliquots in series. To evaluate device performance under punctuated operation, 100 μL aliquots of a 1 mL sample volume were sequentially processed in a single device at a flow rate of 10 μL min^{-1} for 10 min each (Fig. 6). The 10 min cycle time serves to avoid significant loss of capture efficiency associated with longer processing periods, as seen in Fig. 3D. Analysis of the EV concentration in each collected fraction shows consistent performance across all runs, with low variability between each collected fraction and cumulative EV recovery that is nearly linear with cycle count, confirming reproducible enrichment for the full 1 mL sample. This result demonstrates that

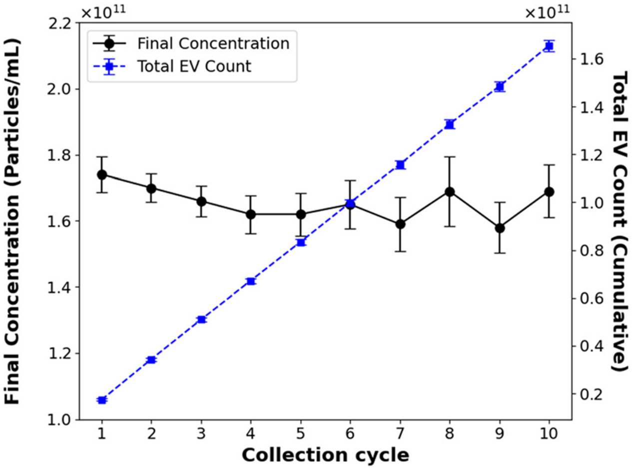

Fig. 6 Punctuated operation of the electrophoretic enrichment device. EV samples were sequentially processed in 100 μL aliquots (Q = 10 μL min^{-1}, t = 10 min per cycle) across 10 consecutive collection cycles.

punctuated operation can serve as a scalable strategy for processing larger input volumes without compromising capture efficiency or reproducibility.

Buffer exchange for pH gradient formation

Following EV concentration and purification using an electrokinetic enrichment chip, the collected vesicles were prepared for pH-gradient–based loading. In the first step, the vesicles were dehydrated with ethanol overnight to remove residual water and then rehydrated in citrate buffer at pH 2.5 for 1 hour to protonate the lipid headgroups and encapsulate the acidic environment as required to establish an internal low-pH compartment. A 4-layer microdialysis chip (Fig. 7) was then employed using HBS at pH 9.4 as a counterflow buffer to form a transmembrane pH gradient suitable for active loading of drug cargo into the vesicles. Counterflow channels were maintained at equal flow rates of 20 μL min^{-1} in opposite directions, consistent with our previously reported operating conditions.[57] Replicate runs confirmed reproducible buffer exchange performance, with negligible variation observed in buffer pH, vesicle size distribution, or vesicle concentration.

Therapeutic loading within the processed vesicles was characterized using AO, an amphipathic weak base commonly used as a model agent to evaluate ion-gradient drug loading that has also been investigated as an exosome-based theranostic agent for multiple cancers.[65] Following incubation of EVs with AO, the measured encapsulation efficiency of AO within the enriched and pH gradient-modified vesicles was found to be 89 ± 3% (mean ± SD, n = 3). This high encapsulation efficiency confirms the formation of a steep transmembrane pH gradient during counterflow microdialysis, leading to efficient protonation and aggregation of drug within the vesicles. The low variance among replicates further indicates high reproducibility for the overall loading process, demonstrating that the pH-gradient-based approach enables robust and consistent encapsulation within the enriched vesicles.

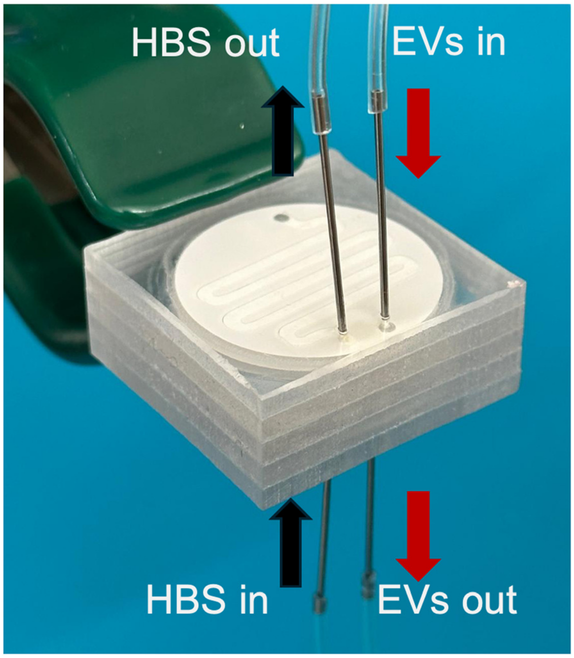

Fig. 7 Multilayer microfluidic counterflow dialysis chip for continuous buffer exchange.

To confirm that EVs retain functional bioactivity after processing through the full electrokinetic concentration and pH-gradient buffer exchange, a TNF-α suppression assay was conducted using LPS-stimulated RAW264.7 macrophages (Fig. 8). LPS was used to induce a controlled inflammatory response, serving as a standard model for assessing anti-inflammatory efficacy of the processed EVs. Vesicles were isolated, purified, and conditioned using the microfluidic devices were administered at three dose levels: 1 × 10^{8}, 1 × 10^{9}, and 1 × 10^{10} particles. Compared to the control group that lacked EV exposure (no treatment), which exhibited elevated TNF-α secretion (~43 000 pg mL^{-1}), all EV pretreatment groups significantly suppressed proinflammatory cytokine production in a dose-dependent manner. EV at doses of 1 × 10^{9}, and 1 × 10^{10} particles resulted in robust reductions, with the 1 × 10^{10} particles achieving near-complete suppression comparable to the positive control (dexamethasone-treated group). Notably, TNF-α levels in the 10^{10} EV group approached basal levels observed in the untreated media group, confirming strong anti-inflammatory effects. The clear dose–response indicates that EVs processed

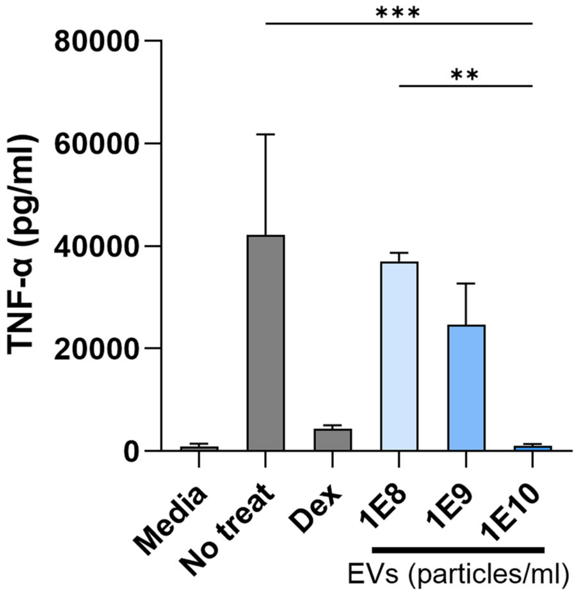

Fig. 8 Bioactivity assay evaluating the anti-inflammatory effects of EVs processed through electrokinetic concentration and pH-gradient buffer exchange. EVs were derived from MSC-conditioned media and tested for their ability to suppress LPS-induced TNF-α production in RAW264.7 macrophages. Experimental groups included untreated media, LPS-stimulated (no treatment) control, dexamethasone-treated media, and EV pretreatments at doses of 1 × 10^{8} particles, 1 × 10^{9} particles, and 1 × 10^{10} particles. All values were expressed as mean ± standard deviation (**$p < 0.01$, ***$p < 0.001$).

through the electrophoretic concentration and purification steps followed by pH-gradient buffer exchange remain biologically active and functionally intact, and retain their immunomodulatory function.

Conclusion

The use of electrophoretic enrichment and counterflow microdialysis offers a modular approach to EV-based drug preparation, combining efficient and scalable isolation of purified vesicles from cell culture supernatant with continuous-flow buffer exchange for downstream drug loading *via* pH gradient-based encapsulation of therapeutic molecules within the vesicles. By operating the electrophoretic enrichment process in a punctuated mode, the technology supports the continuous concentration of EVs from large initial sample volumes. Similarly, the counterflow microdialysis technology provides an effective tool for continuous-flow buffer exchange, enabling rapid pH shifting to be performed prior to drug incubation. Both thermoplastic components are manufactured using off-the-shelf membranes that ensure reliable operation in a compact footprint. The combined system has been confirmed to preserve vesicle integrity and bioactivity, making the process well suited for use in translational applications. While the platform was developed and validated for applications in EV-based drug development using vesicles harvested from cell culture, it may be possible to adapt the modular design to process more complex biological matrices such as blood plasma, urine, or cerebrospinal fluid, thereby extending its potential for both diagnostic and therapeutic use. A limitation of the presented approach is the need for vesicle dehydration and rehydration to be performed manually prior to buffer exchange, preventing seamless coupling of the upstream isolation and downstream drug loading processes in the current implementation. Future efforts to integrate these intermediate steps are expected to enable fully automated and scalable manufacturing of EV therapeutics using the microfluidic-enabled technology.

Conflicts of interest

There are no conflicts to declare.

Data availability

The data underlying the presented results are available within the article and its supplementary information (SI). Supplementary information is available. See DOI: https://doi.org/10.1039/d5lc00870k.

Acknowledgements

This work was supported by the National Institutes of Health through grant R21HL159590.

References

1 N. L. Klyachko, C. J. Arzt, S. M. Li, O. A. Gololobova and E. V. Batrakova, *Pharmaceutics*, 2020, **12**, 1171.
2 D. Buschmann, V. Mussack and J. B. Byrd, *Adv. Drug Delivery Rev.*, 2021, **174**, 348–368.
3 K. Cheng and R. Kalluri, *Extracellular Vesicle*, 2023, **2**, 100029.
4 R. E. Lane, D. Korbie, M. Trau and M. M. Hill, *Methods Mol. Biol.*, 2017, **1660**, 111–130.
5 P. Zhang, J. C. Yeo and C. T. Lim, *SLAS Technol.*, 2019, **24**, 477–488.
6 B. Vestad, A. Llorente, A. Neurauter, S. Phuyal, B. Kierulf, P. Kierulf, T. Skotland, K. Sandvig, K. B. F. Haug and R. Øvstebø, *J. Extracell. Vesicles*, 2017, **6**, 1344087.
7 Y. Huang, S. Wang, Q. Cai and H. Jin, *J. Integr. Plant Biol.*, 2021, **63**, 2020–2030.
8 Y. Han, T. W. Jones, S. Dutta, Y. Zhu, X. Wang, S. P. Narayanan, S. C. Fagan and D. Zhang, *Processes*, 2021, **9**, 356.
9 C. Chen, M. Sun, J. Wang, L. Su, J. Lin and X. Yan, *J. Extracell. Vesicles*, 2021, **10**, e12163.
10 J. Rädler, D. Gupta, A. Zickler and S. EL Andaloussi, *Mol. Ther.*, 2023, **31**, 1231–1250.
11 E. R. Dellar, C. Hill, G. E. Melling, D. R. Carter, L. Alberto Baena-Lopez and C. R. Elizabeth Dellar, *J. Extracell. Biol.*, 2022, **1**, e40.
12 F. Momen-Heravi, *Isolation of Extracellular Vesicles by Ultracentrifugation*, Springer New York, New York, NY, 2017, vol. 1660.
13 L. Musante, D. Tataruch-Weinert, D. Kerjaschki, M. Henry, P. Meleady and H. Holthofer, *J. Extracell. Vesicles*, 2017, **6**, 1267896.
14 E. Tomiyama, K. Fujita and N. Nonomura, *Methods Mol. Biol.*, 2021, **2292**, 173–181.
15 Z. Han, C. Peng, J. Yi, D. Zhang, L. Qiao, W. Chen, X. Zhang, J. Wu, Z. Wang, M. Chen and J. Wang, *Sens. Actuators, B*, 2021, **333**, 129563.
16 M. Chen, S. Lin, C. Zhou, D. Cui, H. Haick and N. Tang, *Adv. Healthcare Mater.*, 2023, **12**, e2202437.
17 M. Monguió-Tortajada, C. Gálvez-Montón, A. Bayes-Genis, S. Roura and F. E. Borràs, *Cell. Mol. Life Sci.*, 2019, **76**, 2369–2382.
18 M. Kosanović, B. Milutinović, S. Goč, N. Mitić and M. Janković, *BioTechniques*, 2017, **63**, 65–71.
19 G. Ströhle, J. Gan and H. Li, *Anal. Bioanal. Chem.*, 2022, **414**, 7051–7067.
20 E. Rohde, K. Pachler and M. Gimona, *Cytotherapy*, 2019, **21**, 581–592.
21 Z. Zhao, H. Wijerathne, A. K. Godwin and S. A. Soper, *Extracell. Vesicles Circ. Nucleic Acids*, 2021, **2**, 80.
22 M. Y. Konoshenko, E. A. Lekchnov, A. V. Vlassov and P. P. Laktionov, *BioMed Res. Int.*, 2018, **2018**, 8545347.
23 S. Busatto, G. Vilanilam, T. Ticer, W. L. Lin, D. W. Dickson, S. Shapiro, P. Bergese and J. Wolfram, *Cell*, 2018, **7**, 273.

24 V. Solovicová, A. Ďatková, T. Bertók, P. Kasák, A. Vikartovská, L. Lorencová and J. Tkac, *Microchim. Acta*, 2025, **192**, 1–38.

25 Z. Zhao, Y. Yang and Y. Zeng, *Lab Chip*, 2016, **16**, 489–496.

26 H. Shao, H. Im, C. M. Castro, X. Breakefield, R. Weissleder and H. Lee, *Chem. Rev.*, 2018, **118**, 1917–1950.

27 M. Mercadal, C. Herrero, O. López-Rodrigo, M. Castells, A. de la Fuente, F. Vigués, L. Bassas and S. Larriba, *Int. J. Mol. Sci.*, 2020, **21**, 1–18.

28 C. Peng, J. Wang, Q. Bao, J. Wang, Z. Liu, J. Wen, W. Zhang and Y. Shen, *Cancer Biomarkers*, 2020, **29**, 373–385.

29 F. J. Ansari, H. A. Tafti, A. Amanzadeh, S. Rabbani, M. A. Shokrgozar, R. Heidari, J. Behroozi, H. Eyni, V. N. Uversky and H. Ghanbari, *Biochem. Biophys. Rep.*, 2024, **38**, 101668.

30 F. Tian, C. Liu, J. Deng and J. Sun, *Acc. Mater. Res.*, 2022, **3**, 498–510.

31 L. Zhu, J. Du, X. Cheng, R. Hu, X. Li, X. Chen and S. Xu, *Anal. Chem.*, 2025, **97**, 4695–4705.

32 Y. Meng, M. Asghari, M. K. Aslan, A. Yilmaz, B. Mateescu, S. Stavrakis and A. J. deMello, *Chem. Eng. J.*, 2021, **404**, 126110.

33 J. T. Smith, B. H. Wunsch, N. Dogra, M. E. Ahsen, K. Lee, K. K. Yadav, R. Weil, M. A. Pereira, J. V. Patel, E. A. Duch, J. M. Papalia, M. F. Lofaro, M. Gupta, A. K. Tewari, C. Cordon-Cardo, G. Stolovitzky and S. M. Gifford, *Lab Chip*, 2018, **18**, 3913–3925.

34 R. J. Gillams, V. Calero, R. Fernandez-Mateo and H. Morgan, *Lab Chip*, 2022, **22**, 3869–3876.

35 X. Dong, J. Chi, L. Zheng, B. Ma, Z. Li, S. Wang, C. Zhao and H. Liu, *Lab Chip*, 2019, **19**, 2897–2904.

36 I. Seder, H. Moon, S. Kang, S. Shin, W. Rhee and S. K. Chip, *Lab Chip*, 2022, **22**, 3699.

37 M. Morani, T. D. Mai, Z. Krupova, G. van Niel, P. Defrenaix and M. Taverna, *TrAC, Trends Anal. Chem.*, 2021, **135**, 116179.

38 S. D. Ibsen, J. Wright, J. M. Lewis, S. Kim, S. Y. Ko, J. Ong, S. Manouchehri, A. Vyas, J. Akers, C. C. Chen, B. S. Carter, S. C. Esener and M. J. Heller, *ACS Nano*, 2017, **11**, 6641–6651.

39 J. Sabaté del Río, Y. Son, J. Park, V. Sunkara and Y. K. Cho, *Langmuir*, 2024, **40**, 25772–25784.

40 M. Tayebi, D. Yang, D. J. Collins and Y. Ai, *Nano Lett.*, 2021, **21**, 6835–6842.

41 D. Wang, S. Yang, N. Wang, H. Guo, S. Feng, Y. Luo and J. Zhao, *Biosensors*, 2024, **14**, 174.

42 K. Mogi, K. Hayashida and T. Yamamoto, *Anal. Sci.*, 2018, **34**, 875–880.

43 S. Marczak, K. Richards, Z. Ramshani, E. Smith, S. Senapati, R. Hill, D. B. Go and H. C. Chang, *Electrophoresis*, 2018, **39**, 2029–2038.

44 L. S. Cheung, S. Sahloul, A. Orozaliev and Y.-A. Song, *Micromachines*, 2018, **9**, 306–318.

45 J. Kim, S. Sahloul, A. Orozaliev, V. Q. Do, V. S. Pham, D. Martins, X. Wei, R. Levicky and Y. A. Song, *IEEE Nanotechnol. Mag.*, 2020, **14**, 18–34.

46 R. T. Davies, J. Kim, S. C. Jang, E. J. Choi, Y. S. Gho and J. Park, *Lab Chip*, 2012, **12**, 5202–5210.

47 S. Cho, W. Jo, Y. Heo, J. Y. Kang, R. Kwak and J. Park, *Sens. Actuators, B*, 2016, **233**, 289–297.

48 D. Buschmann, V. Mussack and J. B. Byrd, *Adv. Drug Delivery Rev.*, 2021, **174**, 348–368.

49 A. J. Lennaárd, D. R. Mamand, R. J. Wiklander, S. E. L. Andaloussi and O. P. B. Wiklander, *Pharmaceutics*, 2022, **14**, 38.

50 J. Gao, X. Dong and Z. Wang, *Methods*, 2020, **177**, 114–125.

51 S. A. A. Kooijmans, S. Stremersch, K. Braeckmans, S. C. De Smedt, A. Hendrix, M. J. A. Wood, R. M. Schiffelers, K. Raemdonck and P. Vader, *J. Controlled Release*, 2013, **172**, 229–238.

52 T. N. Lamichhane, A. Jeyaram, D. B. Patel, B. Parajuli, N. K. Livingston, N. Arumugasaamy, J. S. Schardt and S. M. Jay, *Cell. Mol. Bioeng.*, 2016, **9**, 315–324.

53 S. M. Kronstadt, S. M. Jay and A. Jeyaram, *Methods Mol. Biol.*, 2022, **2504**, 231–239.

54 D. B. Fenske and P. R. Cullis, *Encapsulation of Drugs Within Liposomes by pH-Gradient Techniques*, CRC Press, 3rd edn, 2006, vol. 11.

55 N. Dos Santos, K. A. Cox, C. A. McKenzie, F. Van Baarda, R. C. Gallagher, G. Karlsson, K. Edwards, L. D. Mayer, C. Allen and M. B. Bally, *Biochim. Biophys. Acta, Biomembr.*, 2004, **1661**, 47–60.

56 A. Jeyaram, T. N. Lamichhane, S. Wang, L. Zou, E. Dahal, S. M. Kronstadt, D. Levy, B. Parajuli, D. R. Knudsen, W. Chao and S. M. Jay, *Mol. Ther.*, 2020, **28**, 975–985.

57 S. Mehraji and D. L. DeVoe, *Anal. Chem.*, 2025, **97**, 15502–15509.

58 S. Hallal, Á. Tűzesi, G. E. Grau, M. E. Buckland and K. L. Alexander, *J. Extracell. Vesicles*, 2022, **11**, e12260.

59 M. Paulaitis, K. Agarwal and P. Nana-Sinkam, *Langmuir*, 2018, **34**, 9387–9393.

60 G. Raposo and W. Stoorvogel, *J. Cell Biol.*, 2013, **200**, 373–383.

61 E. Schulz, A. Karagianni, M. Koch and G. Fuhrmann, *Eur. J. Pharm. Biopharm.*, 2020, **146**, 55–63.

62 J. Kowal, G. Arras, M. Colombo, M. Jouve, J. P. Morath, B. Primdal-Bengtson, F. Dingli, D. Loew, M. Tkach and C. Théry, *Proc. Natl. Acad. Sci. U. S. A.*, 2016, **113**, E968–E977.

63 M. A. A. Khan, K. Schoene, J. Cashman, A. Abd El Wahed and U. Truyen, *J. Virol. Methods*, 2022, **310**, 114628.

64 M. Auquière, G. G. Muccioli and A. des Rieux, *J. Extracell. Vesicles*, 2025, **14**, e70097.

65 E. Iessi, M. Logozzi, L. Lugini, T. Azzarito, C. Federici, E. P. Spugnini, D. Mizzoni, R. Di Raimo, D. F. Angelini, L. Battistini, S. Cecchetti and S. Fais, *J. Enzyme Inhib. Med. Chem.*, 2017, **32**, 648.